Supplement of

Development of A Land-River-Ocean Coupled Model for Compound Floods Jointly Caused by Heavy Rainfalls and Storm Surges in Large River Delta Regions

Anyifang Zhang[1] and Xiping Yu[2]

[1] Department of Hydraulic Engineering, Tsinghua University, Beijing, China.
[2] Department of Ocean Science and Engineering, Southern University of Science and Technology, Shenzhen, China.

Correspondence: Xiping Yu (yuxp@sustech.edu.cn)

This supporting information includes 18 figures and one table.

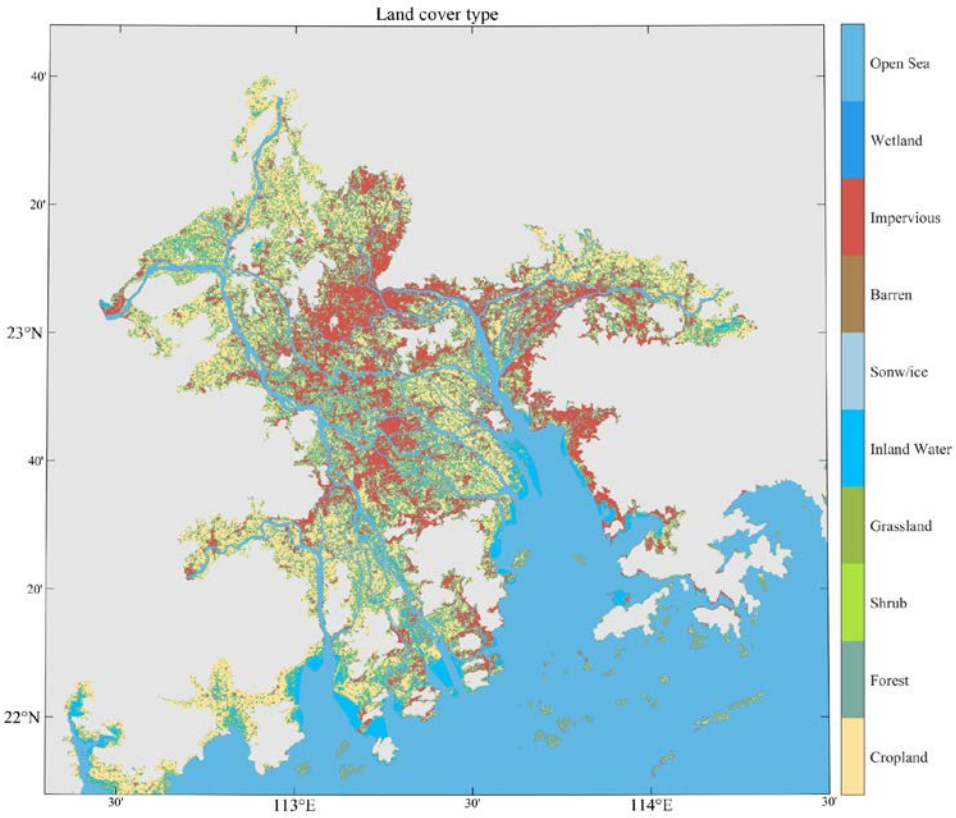

Figure S1. Distribution of landcover type in Pearl River delta region.

Table S1. Manning coefficient for different types of land cover.

Type of Land Cover	Maning coefficient
Open sea	0.01
Cropland	0.037
Forest	0.1
Shrub	0.05
Grassland	0.034
Inland Water	0.02
Snow	0.01
Barren	0.09
Impervious	0.15
Wetland	0.01

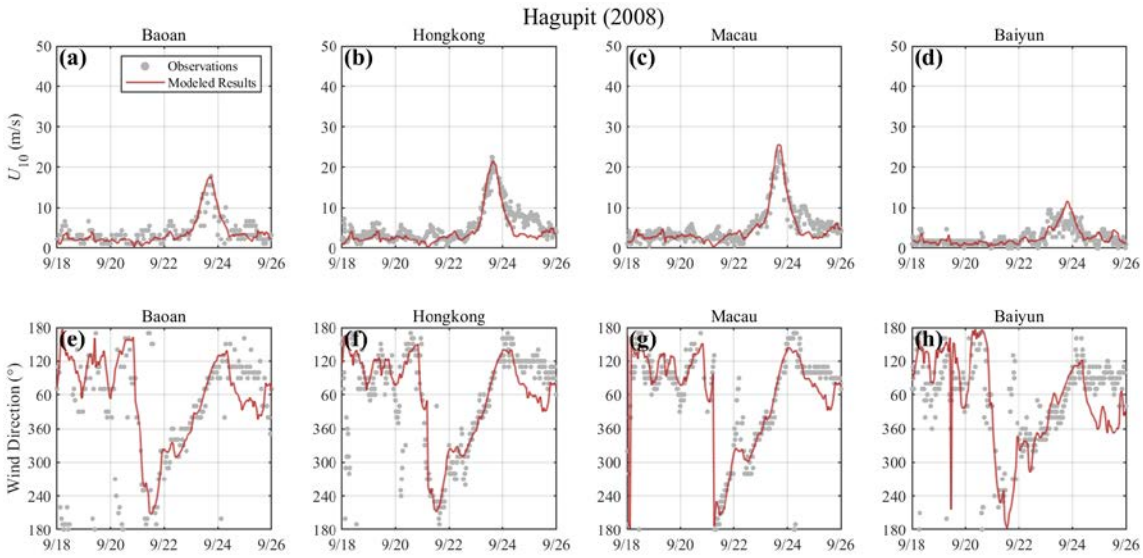

Figure S2. Comparison of computed and observed wind speed and wind direction during Typhoon Hagupit (2008) at four meteorological stations [I. Baoan, II. Hongkong, III. Macau, and IV. Baiyun].

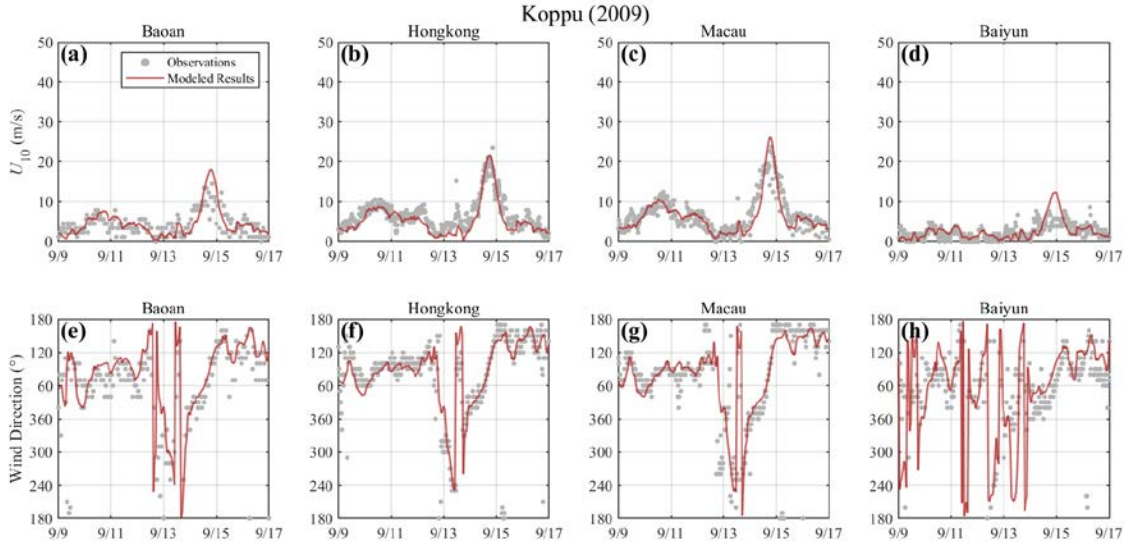

Figure S3. Same as **Figure S2** but during Typhoon Koppu (2009)

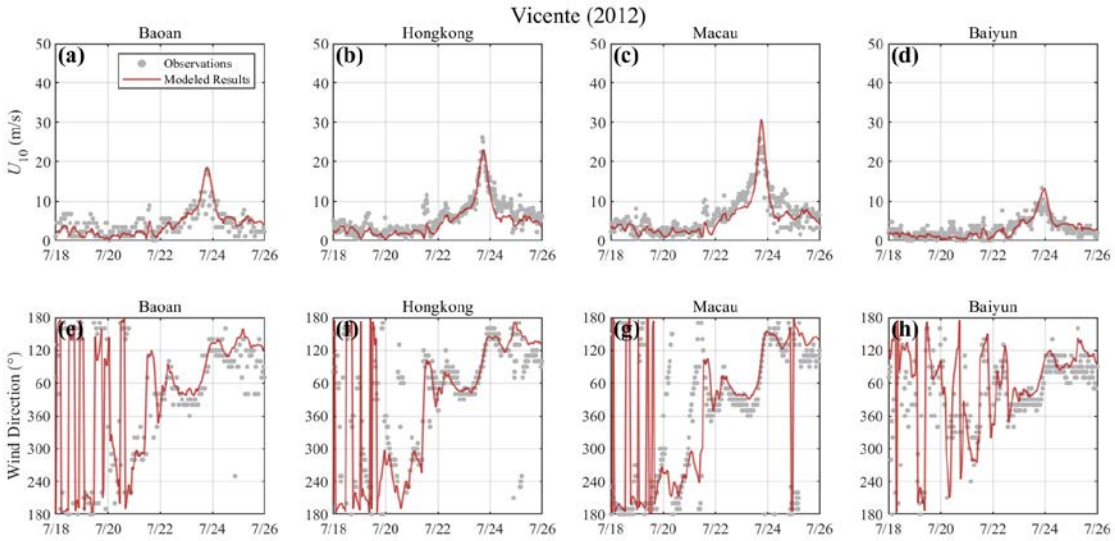

Figure S4. Same as **Figure S2** but during Typhoon Vicente (2012).

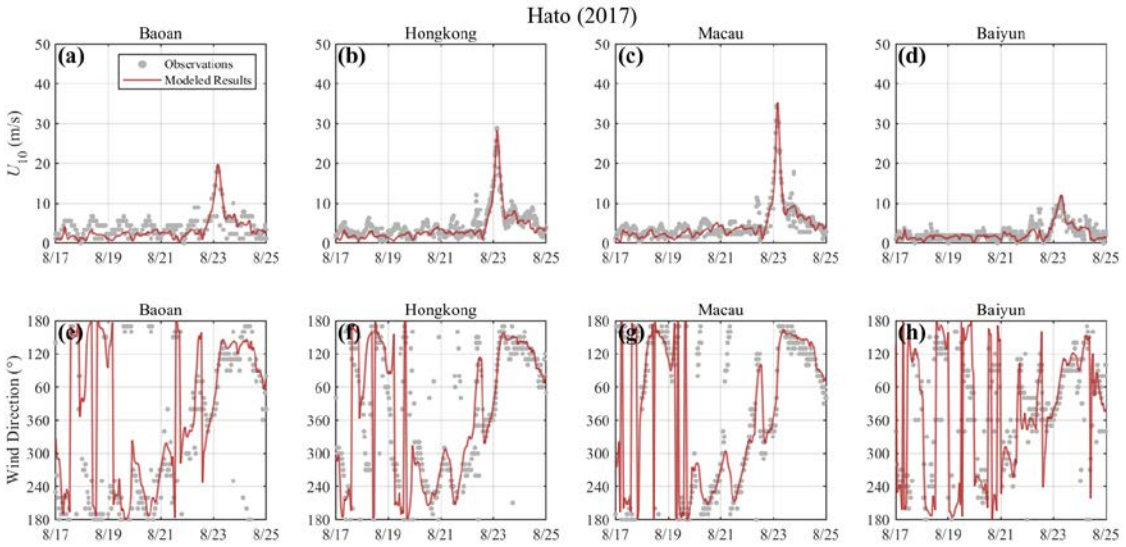

Figure S5. Same as **Figure S2** but during Typhoon Hato (2017).

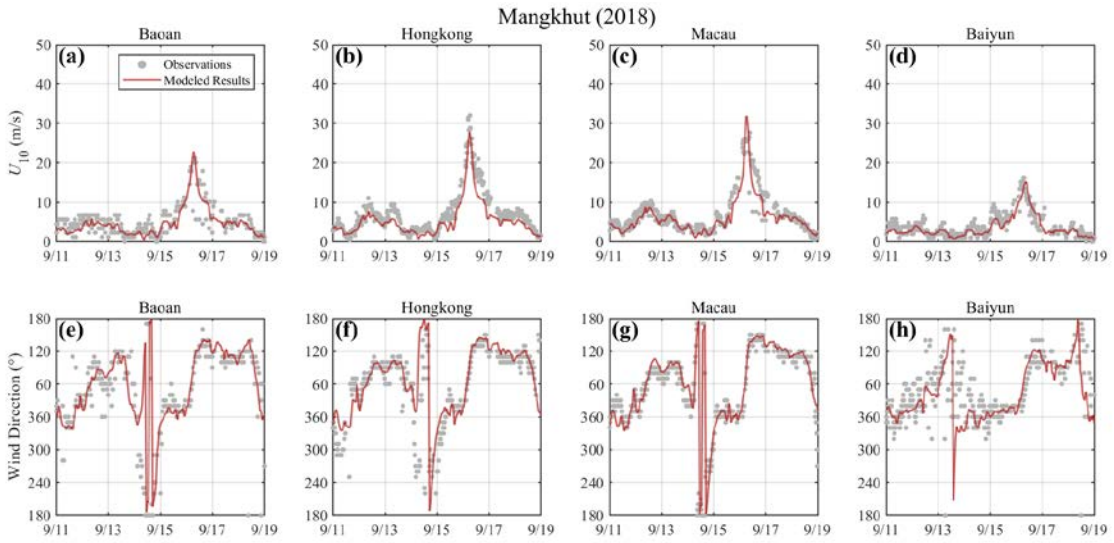

Figure S6. Same as **Figure S2** but during Typhoon Mangkhut (2018).

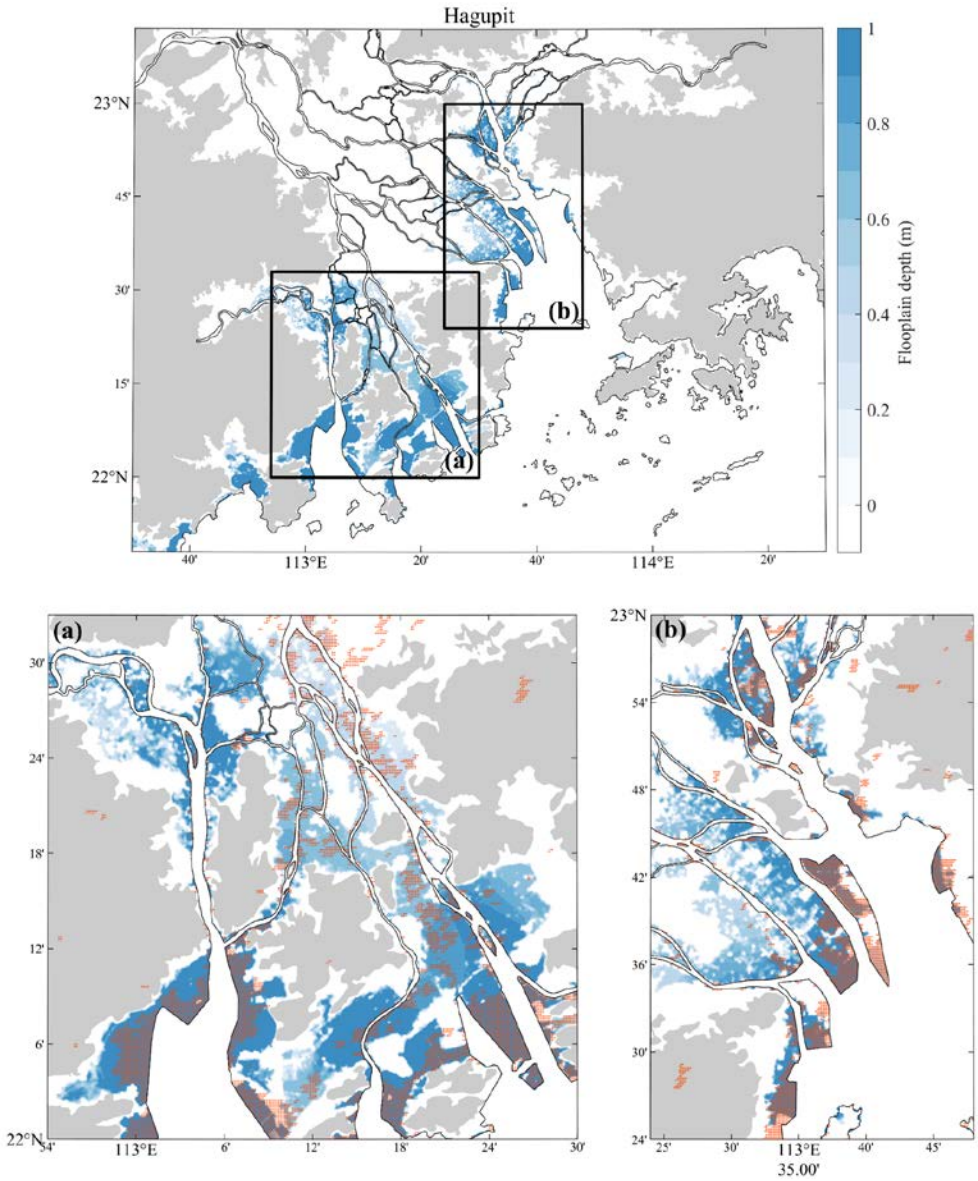

Figure S7. The contour plot (blue) of computed inundation depth caused by Typhoon Hagupit (2008). The orange dots are the inundation range estimated by MODIS datasets.

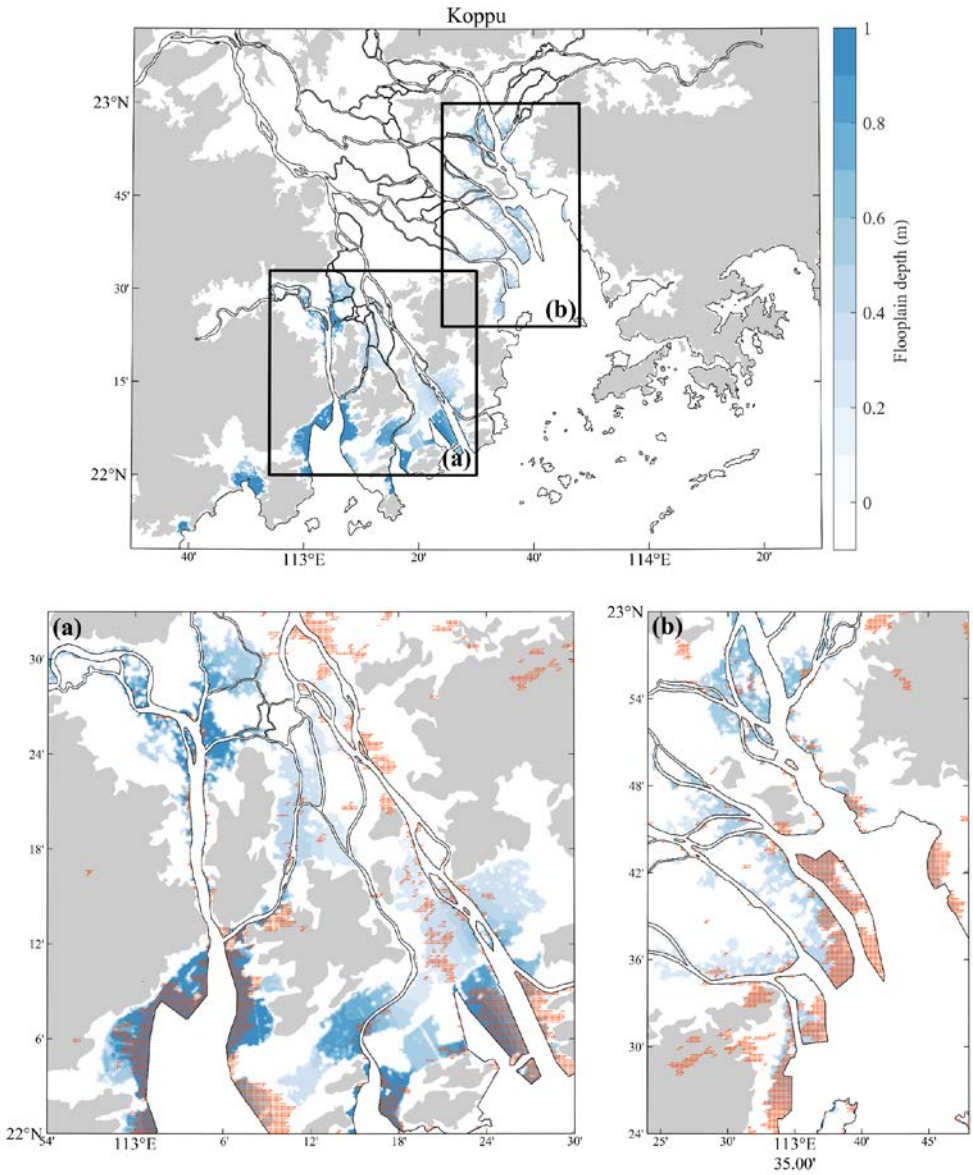

Figure S8. Same as **Figure S7** but caused by Typhoon Koppu (2009).

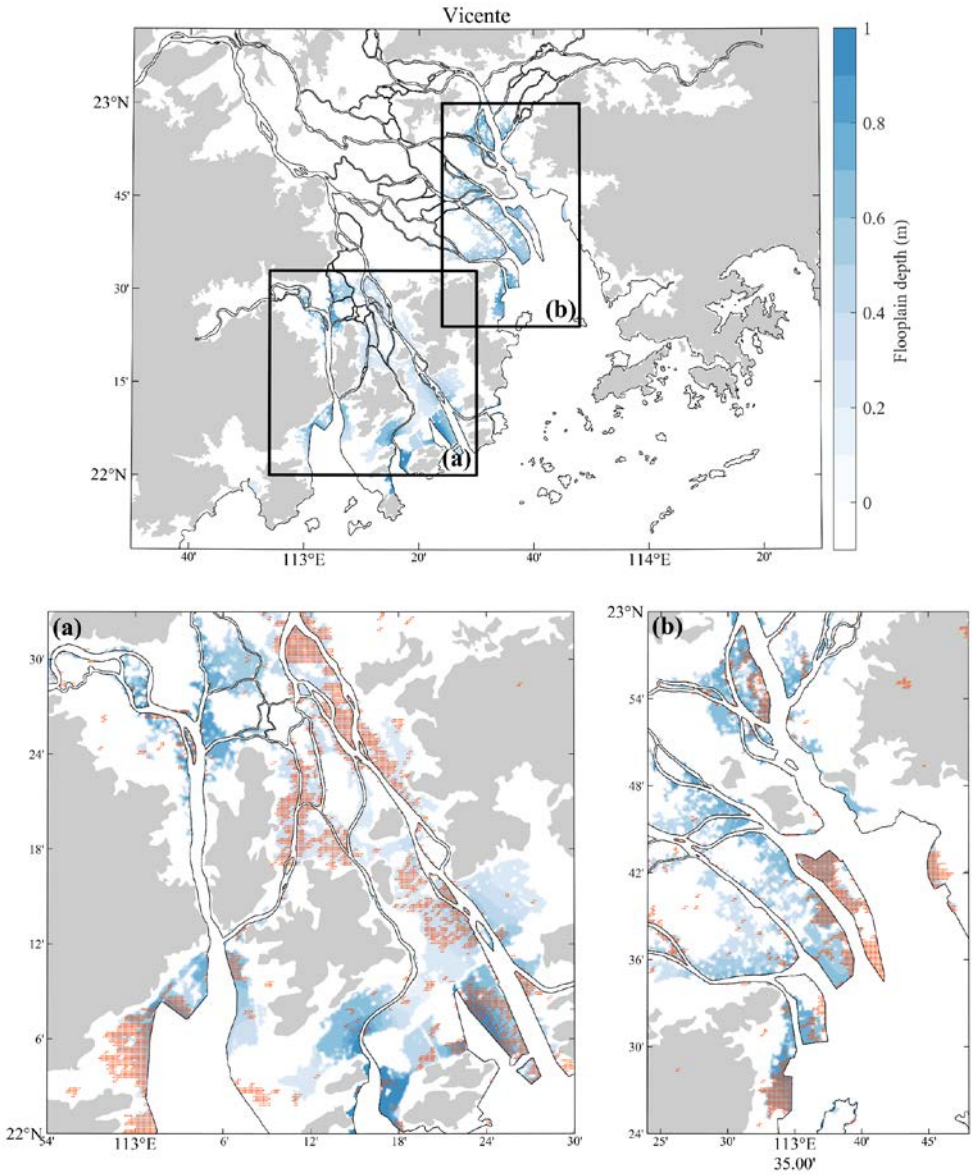

Figure S9. Same as **Figure S7** but caused byTyphoon Vicente (2012).

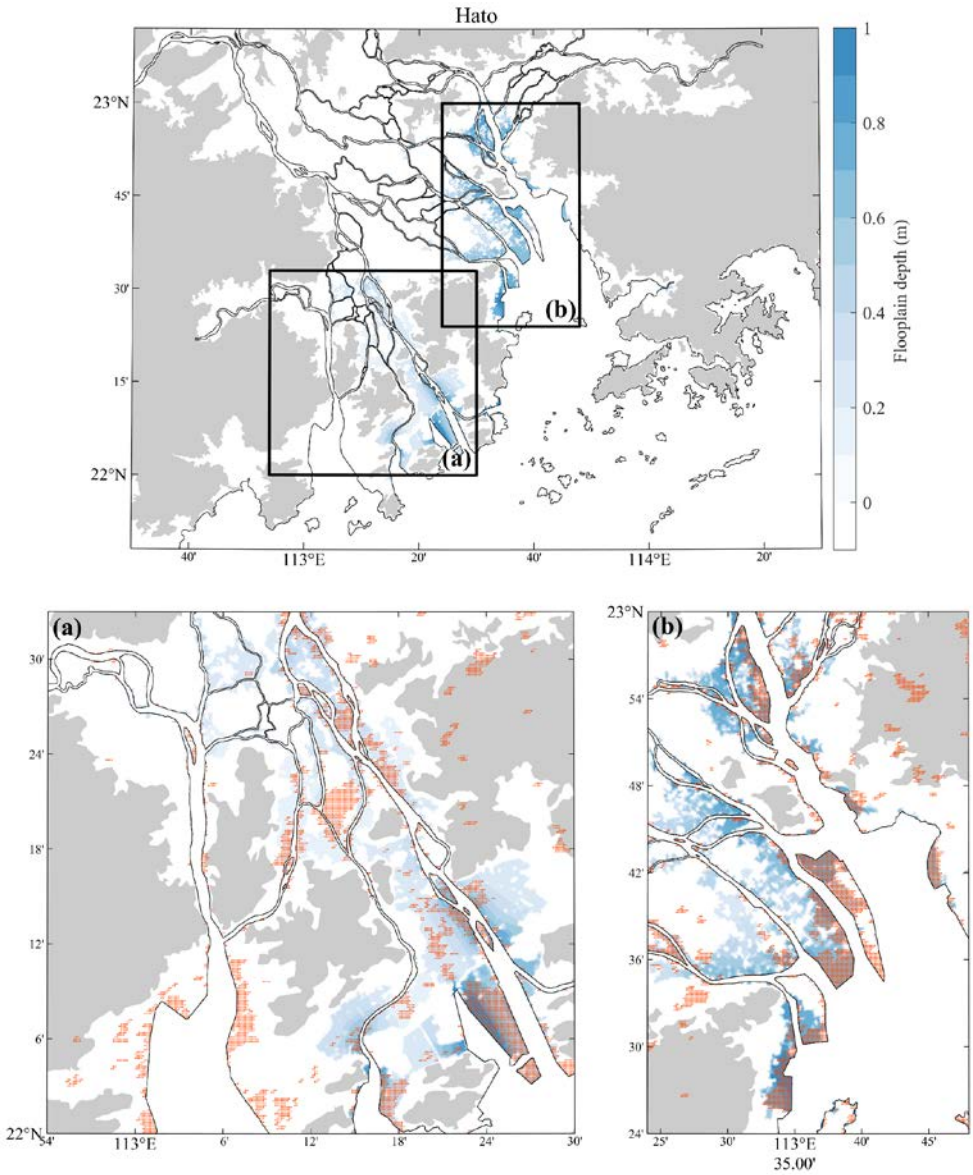

Figure S10. Same as **Figure S7** but for Typhoon Hato (2017).

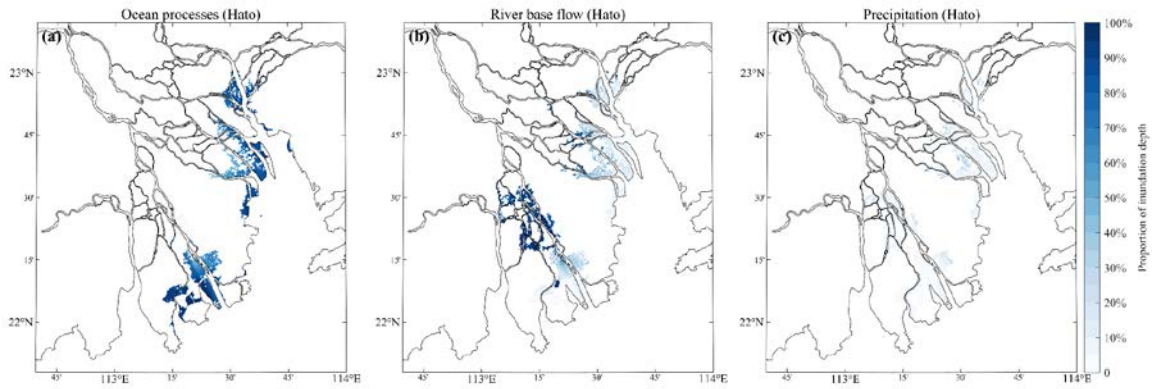

Figure S11. The distribution of inundation depth contributed by (a) the ocean processes, (b) the river base flow, and (c) the precipitation during Typhoon Hagupit (2008).

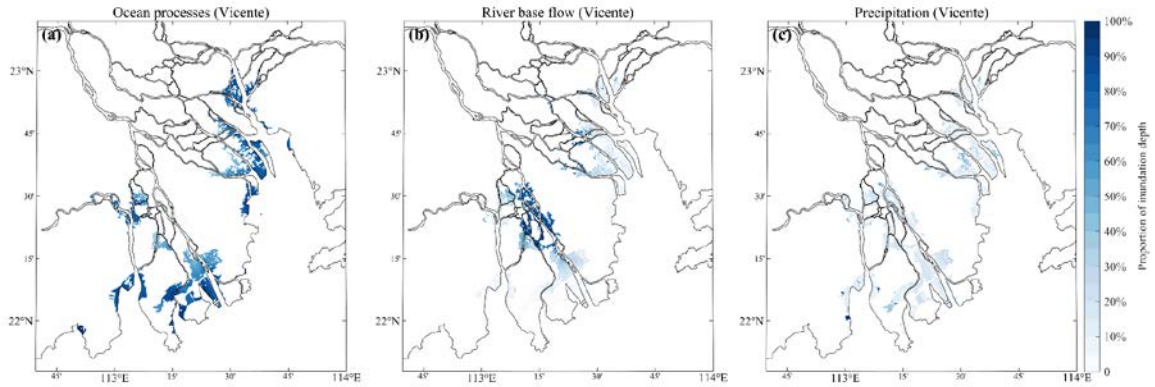

Figure S12. Same as **Figure S11** but during Typhoon Koppu (2009).

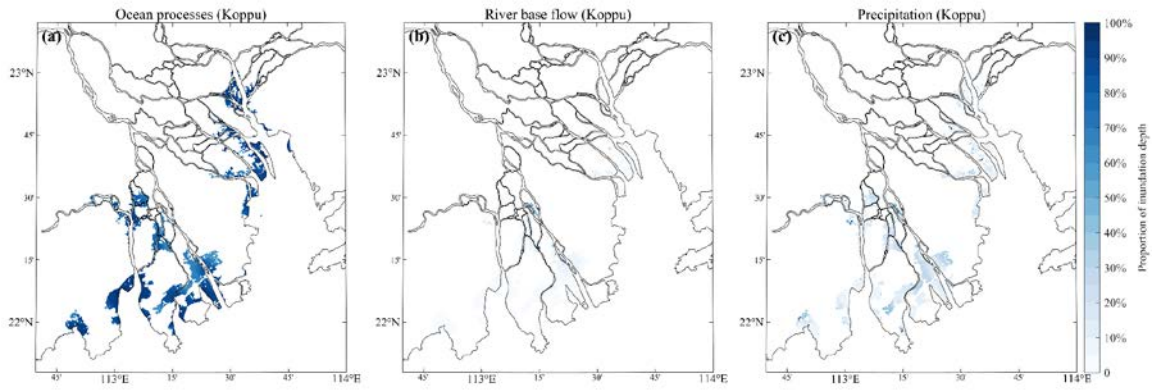

Figure S13. Same as **Figure S11** but during Typhoon Vicente (2012).

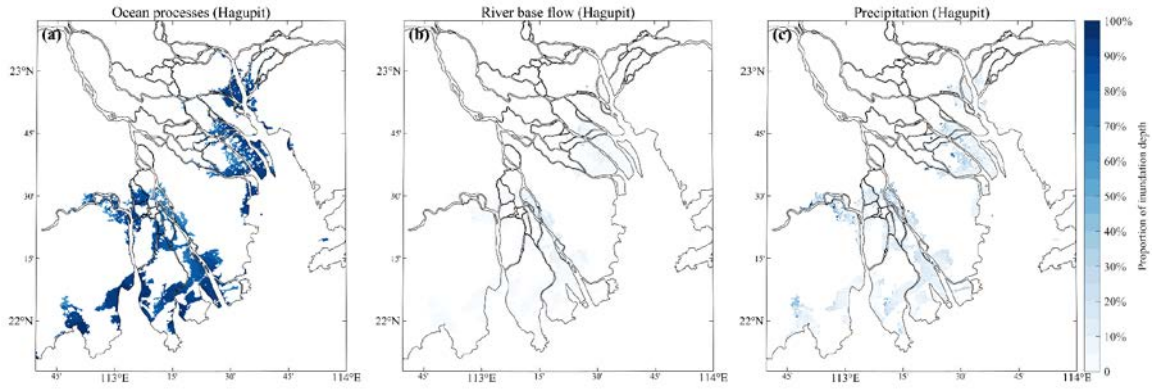

Figure S14. Same as **Figure S11** but during Typhoon Hato (2017).

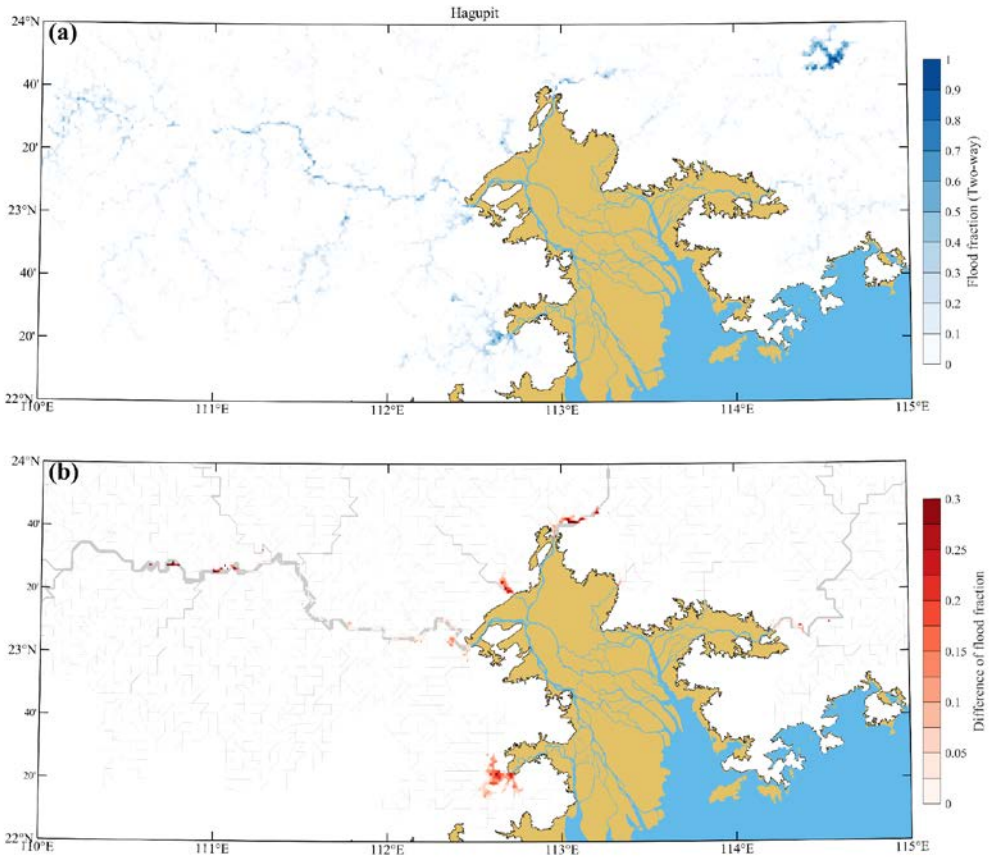

Figure S15. (a) The fraction of flooding area during Typhoon Hagupit (2008) estimated by the CaMa-flood model with two-way coupling approach. **(b)** The difference of the fraction of flooding area between the two-way and one-way coupling approaches. The river channels are marked with gray lines, with the width of the river channel indicated by the line thickness.

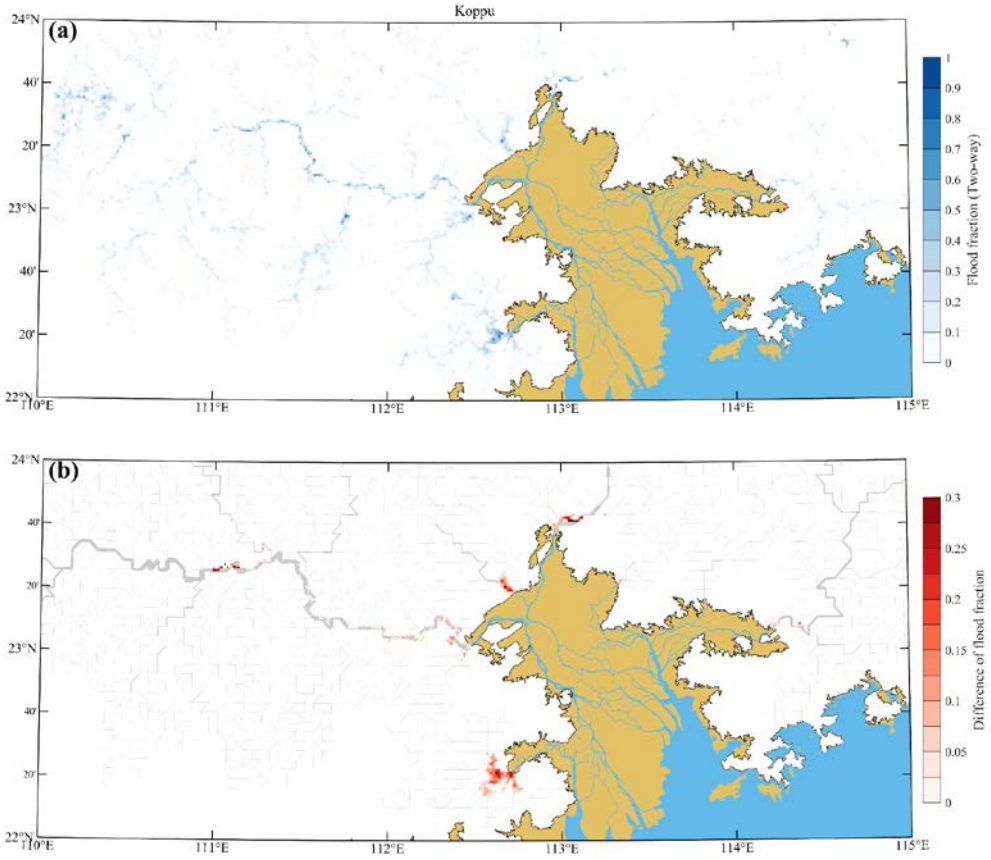

Figure S16. Same as **Figure S15** but during Typhoon Koppu (2009).

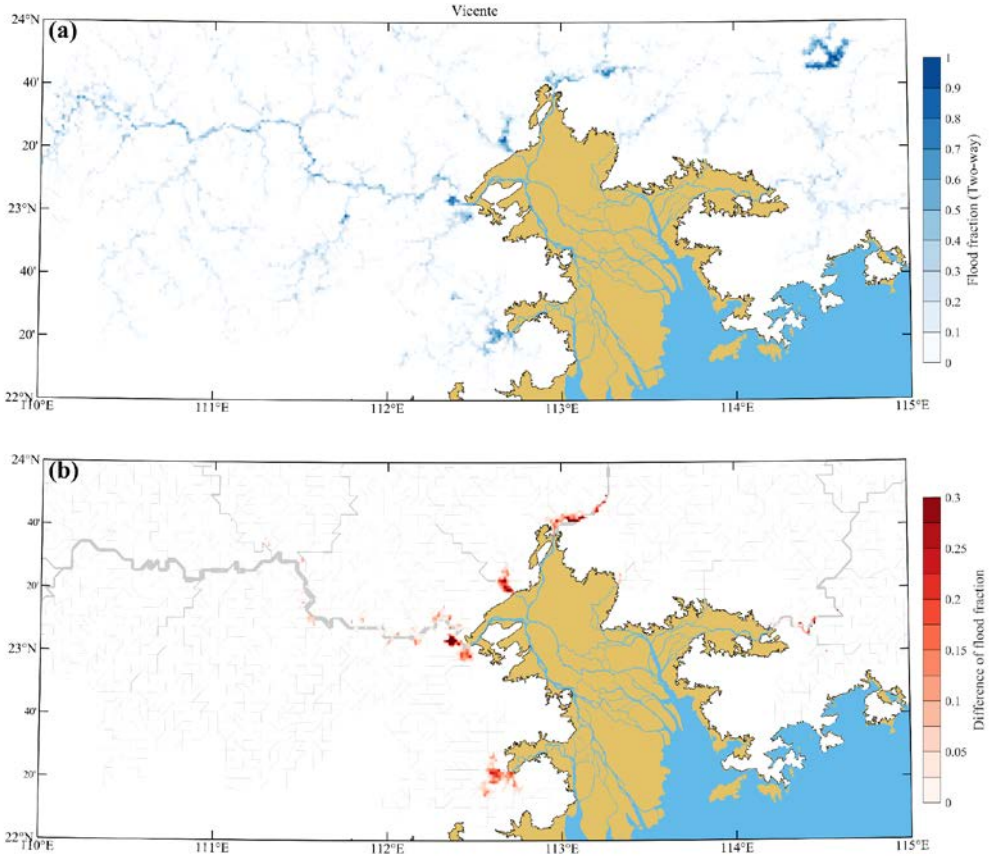

Figure S17. Same as **Figure S15** but during Typhoon Vicente (2012).

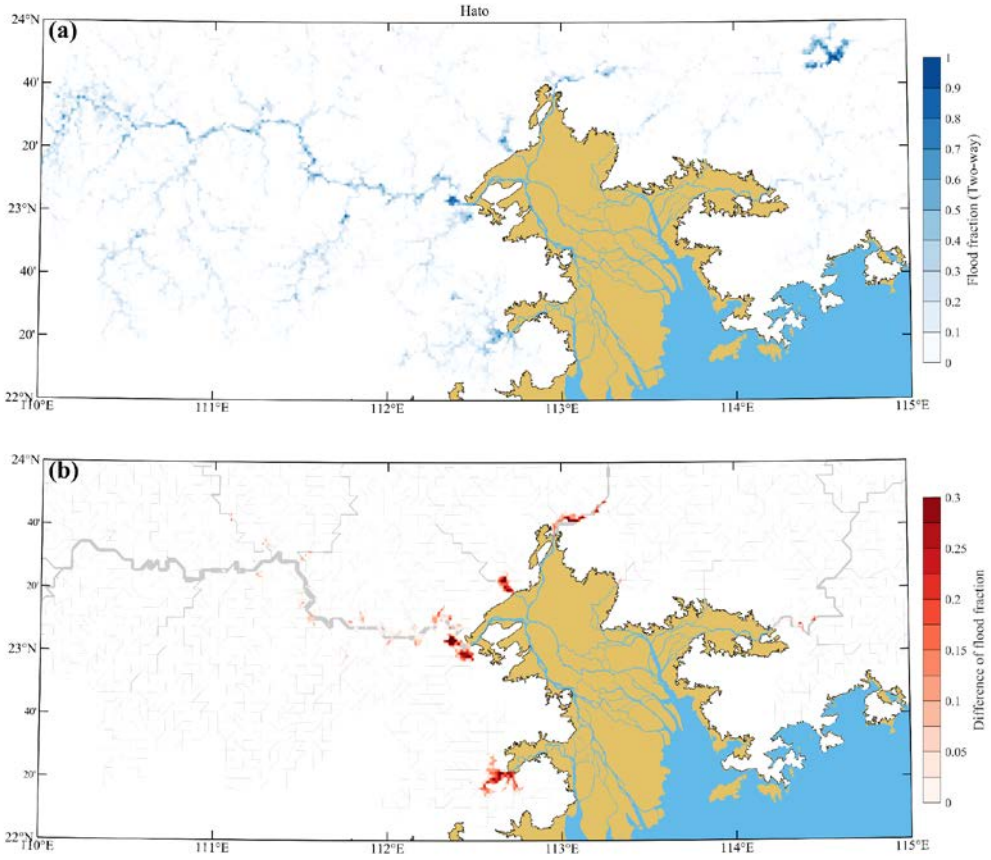

Figure S18. Same as **Figure S15** but for Typhoon Hato (2017).